Eurographics Symposium on Rendering 2022
A. Ghosh and L.-Y. Wei
(Guest Editors)

Volume 41 (2022), Number 4

Microsurface Transformations

A. Atanasov[1,2] V. Koylazov[1] R. Dimov[1] A. Wilkie[2]

[1]Chaos Software, Bulgaria
[2]Charles University, Czech Republic

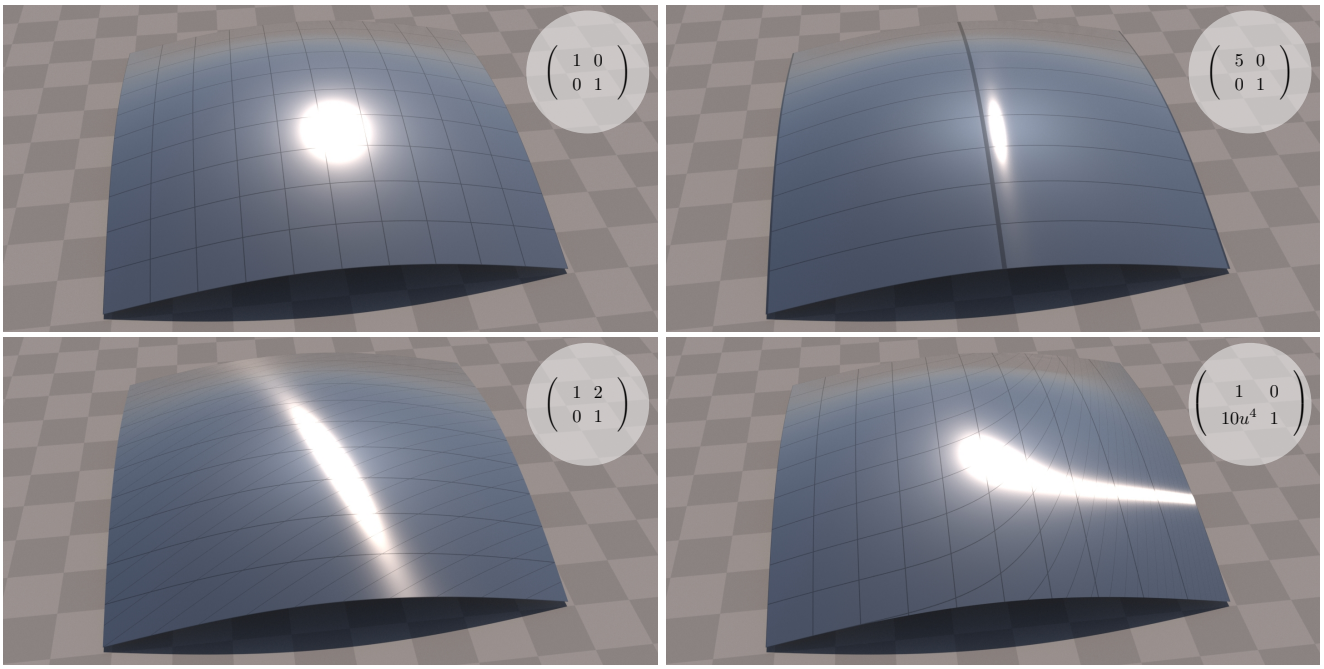

Figure 1: *A demonstration how different 2D transformations (top right insets) of the microsurface affect the reflection off a rough silver plate.* ***Top left:*** *The original unmodified surface with shape-variant GTR distribution with tail* $\gamma = 1.7$ *and roughness* $\alpha = 0.0121$*. A* 10×10 *grid covers the unit texture space to serve as a reference.* ***Top right:*** *The microsurface is stretched* 5 *times horizontally. This makes the surface smoother in that direction, so the highlight is compressed accordingly.* ***Bottom left:*** *A skew transform M with* $(a,b,c,d) = (1,0,2,1)$*, see Equation (9).* ***Bottom right:*** *An example of a non-linear transformation:* $T(u,v) = (u, v+2u^5)$*. The Jacobian matrix* J_T *(top right inset) is a local linear approximation of T and we apply it as a local tangential transform in Equation (9). Notice that the prolonged shape of the highlight to the right is due to more surface compression in that region.*

Abstract

We derive a general result in microfacet theory: given an arbitrary microsurface defined via standard microfacet statistics, we show how to construct the statistics of its linearly transformed counterparts. A common use case of such transformations is to generate anisotropic versions of a given surface. Traditional anisotropic derivations based on varying the roughness of an isotropic distribution in an ellipse have a general closed-form formula only for the subclass of shape-invariant distributions. While our formulation is equivalent to these specific constructs, it is more general in two aspects: it leads to simple closed-form solutions for all distributions, including shape-variant ones, and works for all invertible 2D transform matrices. The latter is of particular importance in case of deformation of the macrosurface, since it can be approximated locally by a linear transformation in the tangent plane. We demonstrate our results using the Generalized Trowbridge-Reitz (GTR) distribution which is shape-invariant only in the special case of the popular Trowbridge-Reitz (GGX) distribution.

CCS Concepts

• ***Computing methodologies*** → ***Rendering; Reflectance modeling;***

1. Introduction

Microfacet theory is based on geometric optics [BS63; TS67] and it has been adopted in computer graphics as a standard technique [Bli77; CT82; WMLT07]. It captures the statistical behavior of rough surfaces: microfacet surfaces (microsurfaces) are represented by a microfacet distribution function and a proper shadowing term is necessary for physically-correct microsurface configurations [Smi67; APS00; Hei14]. A practically viable and physically-based microfacet model requires both analytic formulas for evaluating and sampling the microfacet distribution, and a simple and accurate formula for the shadowing term. Sampling equations for the distribution of visible normals [HD14] are also highly desirable. Unfortunately, they are available only for the two most popular microfacet distributions [RBSM19] - the Beckmann distribution [BS63] and the Trowbridge-Reitz distribution [TR75]. The latter distribution was popularized by Walter et al. [WMLT07] with the alias "GGX". The important effect of multiple scattering in microfacet surfaces has been addressed [HHdD16], but this is out of the scope of our work. We restrict our results to the first scattering event. Also, our work is based entirely in geometric optics, and diffraction effects are ignored [HP17]. Lastly, a model that can be extended to an anisotropic microfacet distribution is valuable in practical applications, as this functionality adds substantial additional control over object appearance, besides the basic parameters of the microfacet distribution function: many real-world objects exhibit anisotropic reflections [Kaj85], so models that are capable of describing their appearance are needed.

The current state of the art for creating analytic anisotropic distributions from existing analytic isotropic ones is based on varying the roughness of the isotropic distribution in an ellipse. This idea can be traced back at least to the elliptical Gaussian model of Ward [War92]. It was later adapted to microfacet models [APS00; KSK10] and has been used since then in modern rendering systems [NVZJ19; PJH16; Bur12]. Heitz defined the class of shape-invariant isotropic distributions for which this construction is always possible [Hei14]. Specifically, this class of distributions has considerable practical advantages:

- Derivation of normalized anisotropic distributions by applying different roughness values in x and y direction. For shape-invariant distributions this is equivalent to a non-uniform scaling of the distribution.
- Extension of the 1D isotropic shadowing function to anisotropic without increasing its dimension.
- Extension of the isotropic sampling equations (including distribution of visible normals if available) to anisotropy.

Our work generalizes all of these advantages to all microfacet distributions and to all 2D invertible transformations, beyond simple scaling. We investigate how the microfacet distribution and the shadowing function of an existing microsurface change when the microsurface is linearly transformed in the tangent plane.

The related previous work is presented in the next section. Necessary preliminary concepts from microfacet theory are provided in Section 3. Our method is derived in Section 4: we first investigate which linear transformations of the microsurface result in valid microsurfaces, then we show how to construct the statistics of the transformed microsurfaces and finally we make the connection of our technique with the classical anisotropy for shape-invariant distributions. In Section 5 we demonstrate our technique by constructing anisotropic modifications of shape-variant distributions. To enable the visualization of deforming objects we show how to track the local deformation of an object using a tension texture.

2. Previous work

Kajiya derived anisotropic reflection models from the equations of electromagnetism [Kaj85]. He pointed out that statistical models are desirable, but the anisotropic integrals are "extremely complex". Poulin proposed an anisotropic model based on sampling microscopic cylinders layered onto the surface [PF90]. Ashikhmin et al. [APS00] introduced various anisotropic models to microfacet theory, and developed matching shadowing equations.

Nagano et al. [NFA*15] studied the complex appearance of human skin under deformation. In addition to the meso-structure detail represented by scanned normal maps they showed that microstructure dynamics play a vital role in the overall appearance. Measurement of skin samples indicated that stretched skin appear shinier while compressed skin have rougher look. They incorporated this measurement data into their shader by blurring the stretched portions of the surface and sharpening the compressed ones. From appearance point of view this aspect is similar to our work, although we present a mathematical framework for microfacet surfaces that is not based on measurements. Dupuy et al. [DHI*13] presented a filtering technique for displaced surfaces based on non-centred anisotropic Beckmann distributions. It is a multi-scale representation for mapped surfaces that, similarly to our work, can predict scaled surface appearance. However, our work is focused on microsurface-related behavior for all distributions while their work is targeted at filtering Beckmann surfaces. Non-centred distributions can be used to modulate an arbitrary microsurface by a normal or displacement map, and they can be applied to our model as well. The shifted distribution remains normalized and only the shadowing function requires alteration [Hei14].

There are a number of approaches for filtering reflectance from microstructures [HSRG07; WDR11; JHY*14; WZYR19], including a large amount of work for rendering glints following the framework of Yan et al. [YHJ*14]. A model capable of large spectrum of appearances based on tabulated piecewise linear distributions was presented by Ribardière et al. [RBSM19]. Our work is targeted at modifying existing distributions and as such is orthogonal to these methods.

GGX is probably the microfacet distribution that is currently most widely used in practice, as it has been consistently verified to be a better all-around match for acquired data [TR75; Bli77; WMLT07; DHI*15] than the Beckmann distribution: the main reason for this seems to be the long tails of the distribution. However, many real materials have even longer tails, and therefore Disney developed the Generalized Trowbridge-Reitz (GTR) distribution as a natural extension to the GGX distribution [Bur12]: this exposes an exponent γ that provides additional control of the tail. This is especially attractive for exponents less than two, which correspond to heavier tails that those of GGX. For example, a GTR exponent $\gamma = \frac{3}{2}$ results in the Henyey-Greenstein distribu-

tion [HG41] evaluated at half-angles, while exponent of $\gamma = 1$ corresponds to the Berry distribution [Ber23] which is employed in the coat layer of Disney's material [Bur12]. We are not aware of other tail-controllable distributions that are used in the industry. Interestingly, the GTR distribution is shape-variant for all tail exponents $\gamma \neq 2$, and the elliptical anisotropic formulation cannot be integrated analytically in these cases [Bur12]. This makes it a practical use case to demonstrate our technique on.

Löw et al. [LKYU12] introduce isotropic models suited for glossy reflections that allow control of the tail of the distribution. Work has been done to develop shape-invariant distributions that admit tail control. The STD [RBMS17] was proposed to span Beckmann and GGX distributions although the heavier than GGX tail control was limited. The Hyper-Cauchy distribution was utilized in the optics literature [WOB*06] and was later used for BRDF fitting [BM14]. Ribardière et al. presented a hierarchical classification of analytic distributions that generalize Beckmann and GGX distributions until they reach the most general Skewed Generalized T-Distribution (SGTD) [RBSM19]. They note that only the distributions in the lower levels of this hierarchy are shape-invariant, and therefore are guaranteed to have an anisotropic form. With our framework an anisotropic version of any SGTD can easily be constructed. Notably, the GTR distribution is not part of this classification. Recently, Barla et al. [BPV18] presented a technique that combines two BRDFs to provide more control on the tails of the distribution. Similarly, our technique modifies existing BRDFs and can be employed on top of their technique when their input BRDFs are microfacet-based.

It has been shown that genetic programming could be used to find new analytic BRDFs, including microfacet ones that provide better fits to acquired data compared to existing microfacet BRDFs [BLPW14]. All of their microfacet distributions are isotropic, and it is unlikely for their technique to generate shape-invariant distributions. Our framework can directly extend them to anisotropy.

Heitz et al. [HDHN16] introduced Linearly Transformed Spherical Distributions (LTSD), and derived a closed-form formula for them. However, their formula does not lead to normalized microfacet distributions, while our framework for linearly transformed microsurfaces ensures this. In Section 4, we derive the Jacobian that ensures the normalization of the transformed microfacet distributions, and discuss the differences to the LTSD formulation.

Finally, there are examples of shape-variant distributions used in the industry, like Phong [WMLT07], Sheen [EK17], discrete GGX and Beckmann [AK16], and GTR [Bur12].

3. Preliminaries

In this section we review the relevant background. The main notation is collected in Table 1.

3.1. Microsurface statistics

In microfacet theory the shaded surface is referred to as the *macrosurface*, while the microscopic details are represented by an infinite collection of microfacets which form a continuous *microsurface* [WMLT07]. Features of the macrosurface are assumed to be much larger than the microfacets, so from the standpoint of the microsurface the macrosurface can be assumed to be locally flat. In our exposition all vectors are in the local frame of the macrosurface, and we assume its local normal as $\mathbf{n} = (0,0,1)$. A differential area $\mathrm{d}A$ on the macrosurface is projected along a direction $\mathbf{v} \in \mathcal{H}^2$ to differential area $(\mathbf{v} \cdot \mathbf{n})\mathrm{d}A$, Figure 2.

Table 1: *Table of notation.*

$\mathcal{H}^2$	Unit hemisphere
$\mathbf{v}$	$(v_x, v_y, v_z) = (\sin\theta_\mathbf{v}\cos\phi_\mathbf{v}, \sin\theta_\mathbf{v}\sin\phi_\mathbf{v}, \cos\theta_\mathbf{v}) \in \mathcal{H}^2$
$\mathbf{n}$	Macrosurface normal $(0,0,1)$
$\mathbf{m}$	Microsurface normal (micro-normal)
D	Microfacet distribution function
$D_\mathbf{v}$	Distribution of visible normals from direction $\mathbf{v}$
G_1	Monodirectional shadowing function
P_{22}	Slope distribution
α	Roughness of the microfacet distribution
α_x, α_y	Roughness values along x and y for anisotropy
γ	Tail falloff of the microfacet distribution
M	Microsurface transformation matrix
D_M	Microfacet distribution of the transformed surface
$D_{\mathbf{v}M}$	Visible normals distribution for the transformed surface
G_{1M}	Shadowing function of the transformed surface
P_{22M}	Slope distribution of the transformed surface

The microsurface is fully determined by its profile (commonly Smith) and microfacet distribution $D(\mathbf{m})$ [Hei14]. The latter is defined in a coordinate system that is aligned with the macrosurface. For a given micro-normal $\mathbf{m} \in \mathcal{H}^2$ it evaluates to the differential area of the microsurface oriented with $\mathbf{m}$. In a valid configuration the area of a non-flat microsurface is always greater than the macrosurface area, and the signed projected area of the microsurface must be equal to the projected area of the macrosurface along an arbitrary direction $\mathbf{v} \in \mathcal{H}^2$ [WMLT07], Figure 2 a). This property enforces a normalization constraint on the microfacet distribution:

$$\int_{\mathcal{H}^2} D(\mathbf{m})(\mathbf{v}\cdot\mathbf{m})\mathrm{d}\mathbf{m} = (\mathbf{v}\cdot\mathbf{n}). \tag{1}$$

Pointwise evaluation of microfacet-based BRDFs requires an auxiliary function derived from $D(\mathbf{m})$. The monodirectional shadowing $G_1(\mathbf{o},\mathbf{m})$ yields the fraction of the microfacets with normals $\mathbf{m}$ that are visible from direction $\mathbf{o}$, Figure 2 b). It is subject to a normalization constraint [Smi67; APS00; Hei14]:

$$\int_{\mathcal{H}^2} D(\mathbf{m})G_1(\mathbf{v},\mathbf{m})\max(0,\mathbf{v}\cdot\mathbf{m})\mathrm{d}\mathbf{m} = (\mathbf{v}\cdot\mathbf{n}). \tag{2}$$

This equation is equivalent to the Weak White Furnace Test for specular microfacets [Hei14] when the integration changes from normals $\mathbf{m}$ to vectors on the sphere $\mathbf{i}$ with $\mathbf{m} = \frac{\mathbf{v}+\mathbf{i}}{||\mathbf{v}+\mathbf{i}||}$ [TS67]. Notice the similarity between the two constraints. The negative projected area from the back-facing microfacets in Equation (1) $(\mathbf{v}\cdot\mathbf{m}) < 0$ is clamped in Equation (2), and instead the shadowing is compensated by the G_1 term. This resemblance is illustrated with the two diagrams in Figure 2.

Microfacet BRDFs require a tool to evaluate what portion of microfacets with normal $\mathbf{m}$ are seen from both the incoming $\mathbf{i}$ and

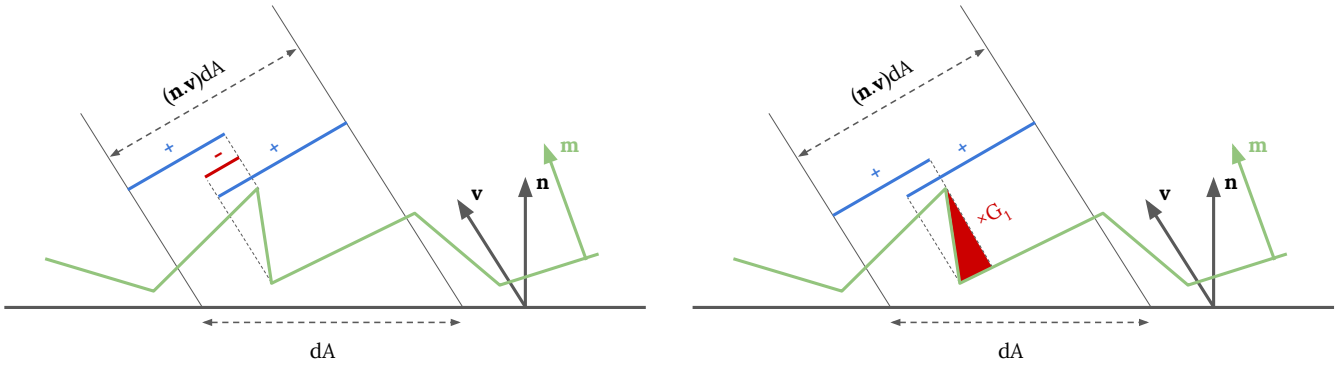

a) Constraint on D, Equation (1) b) Constraint on G_1, Equation (2)

Figure 2: *A differential area* dA *on the macrosurface with normal* $\mathbf{n}$*. The projection of this area along direction* $\mathbf{v} \in \mathcal{H}^2$ *is* $(\mathbf{n}\cdot\mathbf{v})dA$*. The microsurface (green) is continuous and it is composed of microfacets with micro-normals* $\mathbf{m}$*. Microsurface statistics are subject to constraints.* ***a) Microfacet distribution*** *D: The projected areas along* $\mathbf{v}$ *of all forward-facing microfacets (blue) minus the projected areas of all backward-facing microfacets must be equal to the projected area of the macrosurface* $(\mathbf{n}\cdot\mathbf{v})dA$*.* ***b) Shadowing function*** *G_1: When the total projected area along* $\mathbf{v}$ *of forward-facing microfacets (blue) is greater than the projected area of the macrosurface* $(\mathbf{n}\cdot\mathbf{v})dA$ *the shadowing factor G_1 must diminish it to compensate for the shadowed regions (red).*

outgoing $\mathbf{o}$ light directions. This is achieved by the shadowing-masking function $G(\mathbf{o},\mathbf{i},\mathbf{m})$ which is based on the shadowing G_1 [WMLT07; Hei14]. In this paper, we exclusively use the height-correlated shadowing-masking function [RDP05; Hei14].

We use these two constraints to validate our transformed microsurfaces. First we verify that D has a proper normalization. It is sufficient to ensure that the projected microfacets along the macrosurface normal do not overlap and perfectly cover the macrosurface. Hence, Equation (1) is substituted with $\mathbf{v} := \mathbf{n}$:

$$\int_{\mathcal{H}^2} D(\mathbf{m})(\mathbf{n}\cdot\mathbf{m})\mathrm{d}\mathbf{m} = 1. \tag{3}$$

Then to validate G_1 we must ensure that Equation (2) is fulfilled for each $\mathbf{v} \in \mathcal{H}^2$.

Finally, a microfacet distribution can be converted to a distribution of slopes

$$P_{22}\left(-\frac{m_x}{m_z}, -\frac{m_y}{m_z}\right) = D(\mathbf{m})\cos^4\theta_{\mathbf{m}}, \tag{4}$$

where $-\frac{m_x}{m_z}$ and $-\frac{m_y}{m_z}$ are the slopes of a microfacet with normal $\mathbf{m} = (m_x, m_y, m_z)$. The factor $\cos^3\theta_{\mathbf{m}}$ is for the change of measure from solid angle to slopes and the factor $\cos\theta_{\mathbf{m}}$ is for the projection of the microfacets onto the macrosurface [WMLT07; Hei14].

3.2. Anisotropy

The classical anisotropy approach presented here is based on Heitz's extended report [Hei14]. Commonly, microfacet distributions $D(\mathbf{m})$ have roughness parameter to control the spread of the distribution which is usually denoted by α. Traditionally, isotropic distributions are extended to anisotropy by varying the roughness in the xy tangential plane. This is done by specifying roughness α_x along x axis and α_y along y axis and replacing the isotropic argument $\frac{1}{\alpha^2}$ with the ellipse

$$\frac{\cos^2\phi_{\mathbf{m}}}{\alpha_x^2} + \frac{\sin^2\phi_{\mathbf{m}}}{\alpha_y^2}. \tag{5}$$

This leads to a distribution which is not properly normalized. A normalization factor can be computed if Equation (3) can be integrated in closed-form. This is not always possible - for example the GTR distribution does not have closed-form normalization except for the special case of GGX distribution [Bur12].

3.3. Shape-invariant distributions

Shape-invariant isotropic distributions have the property that their shape does not change when the roughness changes. They are an important sub-class of distributions: for all roughness values the distribution curves are scaled copies of each other. Such distributions take the form:

$$D(\mathbf{m}) = \frac{1}{(\mathbf{m}\cdot\mathbf{n})^4}\frac{1}{\alpha^2} f\left(\frac{\tan\theta_{\mathbf{m}}}{\alpha}\right), \tag{6}$$

where the function f is a 1D distribution. The anisotropic version based on Equation (5) is

$$D(\mathbf{m}) = \frac{1}{(\mathbf{m}\cdot\mathbf{n})^4}\frac{1}{\alpha_x\alpha_y} f\left(\tan\theta_{\mathbf{m}}\sqrt{\frac{\cos^2\phi_{\mathbf{m}}}{\alpha_x^2} + \frac{\sin^2\phi_{\mathbf{m}}}{\alpha_y^2}}\right). \tag{7}$$

To complete the anisotropic microsurface configuration the shadowing function $G_1(\mathbf{v},\mathbf{m})$ must be evaluated for the projected roughness onto the direction $\mathbf{v}$

$$\alpha_{\mathbf{v}} = \sqrt{\cos^2\phi_{\mathbf{v}}\alpha_x^2 + \sin^2\phi_{\mathbf{v}}\alpha_y^2}. \tag{8}$$

4. Our framework

We take a different approach to altering microfacet distributions. By investigating how linear transformations of the microsurface af-

fect its statistics we arrive at a simple and general framework for applying modifications to all valid microsurfaces.

4.1. Transforming the microsurface

Although the microfacets are infinitely small, we can still think of the microsurface as a 3D object which is aligned with the macrosurface. For instance, Heitz et al. [HHdD16] validated their multiple scattering model by ray-tracing a pre-generated Beckmann surface. So it stands to reason that the microsurface can be transformed by a 3×3 matrix, just like regular geometry. We consider all such transformations that lead to a valid microsurface. These are all invertible matrices of the form

$$M = \begin{pmatrix} a & c & 0 \\ b & d & 0 \\ 0 & 0 & 1 \end{pmatrix}. \tag{9}$$

- M performs an arbitrary linear transformation on the microsurface in the tangential plane, parallel to the macrosurface, Figure 3 b).
- The first two column vectors of M are restricted to the tangential plane, because the microsurface must remain aligned with the macrosurface, Figure 3 c).
- The first two row vectors of M are also contained in the tangential plane, because vertical shear could break the microsurface configuration. Microfacet normals $\mathbf{m}$ could turn to the negative hemisphere, Figure 3 d).
- Scaling the height of the microsurface h times results in the same microsurface statistics as if we scale the xy plane by a factor of $\frac{1}{h}$. This is observed in the slopes of the transformed surface $-\frac{a\mathbf{m}_x+b\mathbf{m}_y}{\mathbf{m}_z}$ and $-\frac{c\mathbf{m}_x+d\mathbf{m}_y}{\mathbf{m}_z}$ where the scaling of the height $h\mathbf{m}_z$ is identical to modifying M using $(\frac{a}{h}, \frac{b}{h}, \frac{c}{h}, \frac{d}{h})$. Therefore, we always set the last entry of M to 1.

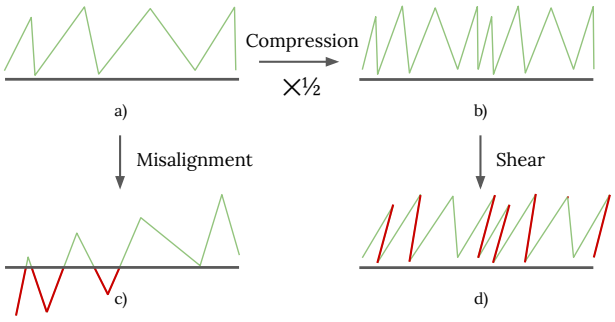

Figure 3: *Valid (top row) and broken (bottom row) microsurface configurations.* ***Compression: a)→ b):*** *Linear transformations parallel to the macrosurface lead to new valid microsurfaces.* ***Misalignment: a)→ c):*** *Linear transformations outside the tangential plane break the micro-macrosurface alignment, as some microfacets sink below the macrosurface (red).* ***Shear: b)→ d):*** *Vertical shear parallel to xy plane moves some microfacets into the negative hemisphere (red).*

A basic fact in computer graphics is that when an object is transformed using a matrix M, the normal vectors to the surface must be transformed by the inverse transpose of that matrix $(M^{-1})^T$. This transformation is derived by enforcing the transformed tangents to be orthogonal to the transformed normals as they should be by definition [PJH16]. Indeed this is directly verified

$$((M^{-1})^T\mathbf{m})^T(M\mathbf{t}) = \mathbf{m}^T(M^{-1}M)\mathbf{t} = \mathbf{m}^T\mathbf{t} = 0, \tag{10}$$

where $\mathbf{t}$ is a tangent to a microfacet with normal $\mathbf{m}$.

Figure 1 demonstrates our method with non-uniform scaling and skew transforms for shape-variant GTR. Note that the effect of stretching in Figure 1 (top right) is observed using the elliptical anisotropic formula for shape-invariant distributions, however in this shape-variant case the linear stretching of the microsurface does not result in linear stretching in the roughness parameter. The effect of a general 2D linear transform in Figure 1 (bottom left) beyond stretching has not been shown so far even for the simpler case of shape-invariant distributions. Furthermore, in Figure 1 (bottom right) we demonstrate our method for a non-linear 2D transformation. The Jacobian matrix of this transformation is a local linear approximation that we use within our framework.

4.2. Statistics of the transformed microsurface

In order to compute the statistics of the transformed microsurface we transform the arguments of the initial valid microsurface statistics. All arguments are unit vectors so a normalization is required after the arguments are transformed.

Shadowing function $G_{1M}(\mathbf{v},\mathbf{m})$: When the vector $\mathbf{v}$ is transformed with the microsurface the shadowing configuration does not change. Note that the micro-normal $\mathbf{m}$ must be transformed with the inverse transpose of M

$$G_{1M}\left(\frac{M\mathbf{v}}{||M\mathbf{v}||}, \frac{(M^{-1})^T\mathbf{m}}{||(M^{-1})^T\mathbf{m}||}\right) = G_1(\mathbf{v},\mathbf{m}), \tag{11}$$

and therefore we can express the shadowing of the transformed microsurface G_{1M} in terms of G_1 by inverting the matrices before the arguments and normalizing

$$G_{1M}(\mathbf{v},\mathbf{m}) = G_1\left(\frac{M^{-1}\mathbf{v}}{||M^{-1}\mathbf{v}||}, \frac{M^T\mathbf{m}}{||M^T\mathbf{m}||}\right). \tag{12}$$

This is a generalization of the masking probability invariance [Hei14]. Indeed, if an object is lit by a directional light and some parts of it are self-shadowed, then a linear transformation applied both to the object and the light direction will preserve the shadowed portions. This is because the linear transformations preserve the projection along the transformed light direction.

Microfacet distribution $D_M(\mathbf{m})$: The input normal $\mathbf{m}$ is transformed similarly, but the resulting distribution is not normalized in general. To find proper normalization we investigate the non-linear transformation $N : \mathcal{H}^2 \to \mathcal{H}^2$ that applies linear transformation to a normal and normalizes the result

$$\mathbf{u} = N(\mathbf{m}) = \frac{M^T\mathbf{m}}{||M^T\mathbf{m}||}. \tag{13}$$

N is a bijection because M^T is invertible. The product of M^T and

the micro-normal $\mathbf{m} = (m_x, m_y, m_z)$ is $M^T\mathbf{m} = (am_x + bm_y, cm_x + dm_y, m_z)$ and has length

$$||M^T\mathbf{m}|| = \sqrt{(am_x + bm_y)^2 + (cm_x + dm_y)^2 + m_z^2}. \tag{14}$$

Note that the microfacet distribution is two-dimensional: the normal $\mathbf{m}$ is on the hemisphere, and can be represented by the first two components m_x and m_y. The z component is projected on the hemisphere $m_z = \sqrt{1 - m_x^2 - m_y^2}$. In order to find a new distribution D_M by transforming the argument of D with N we need to normalize by the absolute value of the Jacobian determinant of N [PJH16]

$$D_M(\mathbf{m}) = |\det J_N| D(\mathbf{u}), \tag{15}$$

where

$$\det J_N = \begin{vmatrix} \frac{\partial u_x}{\partial m_x} & \frac{\partial u_x}{\partial m_y} \\ \frac{\partial u_y}{\partial m_x} & \frac{\partial u_y}{\partial m_y} \end{vmatrix} = \frac{\partial u_x}{\partial m_x}\frac{\partial u_y}{\partial m_y} - \frac{\partial u_x}{\partial m_y}\frac{\partial u_y}{\partial m_x}. \tag{16}$$

We proceed to compute the partial derivatives

$$\frac{\partial u_x}{\partial m_x} = \frac{m_y^2(ad^2 - bcd - a) + m_x m_y(acd + b - bc^2) + a}{||M^T\mathbf{m}||^3} \tag{17}$$

$$\frac{\partial u_x}{\partial m_y} = \frac{m_x^2(bc^2 - acd - b) + m_x m_y(bcd + a - ad^2) + b}{||M^T\mathbf{m}||^3} \tag{18}$$

$$\frac{\partial u_y}{\partial m_x} = \frac{m_y^2(cb^2 - abd - c) + m_x m_y(abc + d - da^2) + c}{||M^T\mathbf{m}||^3} \tag{19}$$

$$\frac{\partial u_y}{\partial m_y} = \frac{m_x^2(da^2 - abc - d) + m_x m_y(abd + c - cb^2) + d}{||M^T\mathbf{m}||^3}. \tag{20}$$

After simplification of Equation (16) using Mathematica [Wol16] we arrive at a concise result

$$\det J_N = \frac{ad - bc}{||M^T\mathbf{m}||^4} = \frac{\det M}{||M^T\mathbf{m}||^4}. \tag{21}$$

We use this result in Equation (15) to obtain the microfacet distribution of the transformed microsurface

$$D_M(\mathbf{m}) = \frac{|\det M|}{||M^T\mathbf{m}||^4} D(\mathbf{u}). \tag{22}$$

We provide geometrical intuition behind Equation (22). The matrix M transforms the xy plane and changes the projected microsurface area by a factor of $|\det M| = |\det M^T|$. The microfacet distribution measures the microsurface differential area relative to the macrosurface differential area, see Figure 4. Therefore, this factor compensates for the change of projected area.

Furthermore, we observe in Figure 5 that

$$||M^T\mathbf{m}|| = \frac{\cos\theta_\mathbf{m}}{\cos\theta_\mathbf{u}}. \tag{23}$$

Therefore, in Equation (22) the factor $\frac{1}{||M^T\mathbf{m}||^4}$ serves the purpose to change the Jacobian $\frac{1}{\cos^3\theta_\mathbf{u}}$ and the inverse projection $\frac{1}{\cos\theta_\mathbf{u}}$ in Equation (4), both with respect to the transformed micro-normal $\mathbf{u}$, to the Jacobian $\frac{1}{\cos^3\theta_\mathbf{m}}$ and the inverse projection $\frac{1}{\cos\theta_\mathbf{m}}$ with respect to the original micro-normal $\mathbf{m}$. Equation (22) is similar to the Linearly Transformed Spherical Distributions (LTSD) [HDHN16], however their formula does not include the inverse projections. Hence, our formulation given with Equations (22) and (9) defines a different family of distributions which we name by analogy Linearly Transformed Microfacet Distributions (LTMD).

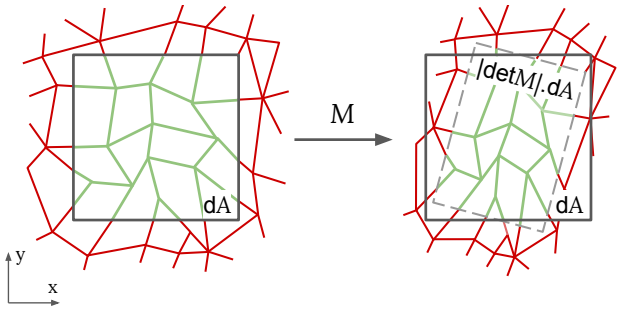

Figure 4: *The microsurface projection onto xy plane.* ***Left:*** *A square patch (black) on the macrosurface has differential* dA*. Portion of the microsurface that is inside this patch is coloured with green while the rest is coloured red.* ***Right:*** *When this microsurface is transformed using the matrix M, the portion of the microsurface which was previously in* dA *is transformed accordingly (gray dashed region). The transform M changes the area by a factor of $|\det M| = |\det M^T|$.*

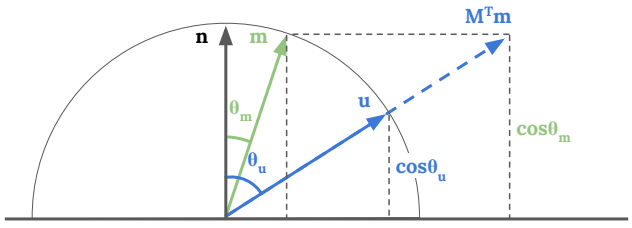

Figure 5: *Geometry of micro-normal transformation. Let* $\mathbf{m}$ *(green) be a micro-normal from the original microsurface. The transformed vector $M^T\mathbf{m}$ (blue, dashed) has the same z-component as the original vector* $\mathbf{m}$ *because the transformation M^T acts only on the xy plane. This vector is normalized and labelled* $\mathbf{u} = \frac{M^T\mathbf{m}}{||M^T\mathbf{m}||}$*. From the two similar right triangles with hypotenuses $M^T\mathbf{m}$ and* $\mathbf{u}$ *we find that* $||M^T\mathbf{m}|| = \frac{\cos\theta_\mathbf{m}}{\cos\theta_\mathbf{u}}$*.*

Finally, we express the slope distribution of the transformed microsurface P_{22M} from the original slope distribution P_{22} by using, in that order, Equations (4), (22) and (23)

$$\begin{aligned} P_{22M}\left(-\frac{m_x}{m_z}, -\frac{m_y}{m_z}\right) &= D_M(\mathbf{m})\cos^4\theta_\mathbf{m} \\ &= \frac{|\det M|}{||M^T\mathbf{m}||^4} D(\mathbf{u})\cos^4\theta_\mathbf{m} \\ &= |\det M|\frac{\cos^4\theta_\mathbf{u}}{\cos^4\theta_\mathbf{m}} D(\mathbf{u})\cos^4\theta_\mathbf{m} \\ &= |\det M| D(\mathbf{u})\cos^4\theta_\mathbf{u} \\ &= |\det M| P_{22}\left(-\frac{u_x}{u_z}, -\frac{u_y}{u_z}\right). \end{aligned} \tag{24}$$

Consequently, Equation (22) can be also derived from the slope distribution.

Sampling micro-normals: in order to implement practical microfacet materials we need sampling equations for the microfacet distribution. In our work we assume that the original microsurface before transformation has sampling equations at least for $D(\mathbf{m})(\mathbf{n}\cdot\mathbf{m})$. Based on these, a micro-normal $\mathbf{u}'$ is sampled

$$\mathbf{u}' \propto D(\mathbf{m})(\mathbf{n}\cdot\mathbf{m}). \tag{25}$$

Then it is transformed to the modified microsurface using the inverse transpose of M

$$\mathbf{m}' = \frac{(M^{-1})^T\mathbf{u}'}{||(M^{-1})^T\mathbf{u}'||} \propto D_M(\mathbf{m})(\mathbf{n}\cdot\mathbf{m}). \tag{26}$$

If the original microfacet distribution has sampling equations for the distribution of visible normals [HD14]

$$D_{\mathbf{v}}(\mathbf{m}) = \frac{G_1(\mathbf{v},\mathbf{m})(\mathbf{v}\cdot\mathbf{m})D(\mathbf{m})}{\mathbf{v}\cdot\mathbf{n}} \tag{27}$$

then we can use them to sample the distribution of visible normals of the transformed surface

$$D_{\mathbf{v}M}(\mathbf{m}) = \frac{G_{1M}(\mathbf{v},\mathbf{m})(\mathbf{v}\cdot\mathbf{m})D_M(\mathbf{m})}{\mathbf{v}\cdot\mathbf{n}}. \tag{28}$$

To do that for a given direction $\mathbf{v}$ we first transform it to the space of the original surface $\mathbf{w} = \frac{M^{-1}\mathbf{v}}{||M^{-1}\mathbf{v}||}$, generate a visible normal $\mathbf{u}'_{\mathbf{w}}$ using the available equations and then transform it to the modified surface using the inverse transpose $\mathbf{m}'_{\mathbf{v}} = \frac{(M^{-1})^T\mathbf{u}'_{\mathbf{w}}}{||(M^{-1})^T\mathbf{u}'_{\mathbf{w}}||}$.

4.3. Numerical validation

In addition to the proof presented in this section we also validated our technique numerically. Specifically, we applied random transformations M on a large variety of microsurfaces with random parameters and verified that:

- The normalization constraint in Equation (3) is fulfilled for all transformed microfacet distributions D_M.
- The shadowing constraint in Equation (2) with random directions $\mathbf{v} \in \mathcal{H}^2$ is fulfilled for all transformed shadowing functions G_{1M}.

The list of tested distributions include GTR [Bur12], anisotropic Beckmann and GGX [Hei14], STD [RBMS17], Phong [WMLT07], Sheen [EK17], Discrete GGX distribution [JHY*14; AK16]. We provide the source code for this numerical validation.

4.4. Equivalence with classical anisotropy for shape-invariant distributions

Suppose that we have a shape-invariant isotropic distribution $D(\mathbf{m})$ with roughness α, defined by Equation (6). To construct the traditional anisotropic form we replace α with two roughness values α_x and α_y and use Equation (7). In our framework this is equivalent to applying the diagonal transformation matrix

$$M = \begin{pmatrix} \frac{\alpha}{\alpha_x} & 0 & 0 \\ 0 & \frac{\alpha}{\alpha_y} & 0 \\ 0 & 0 & 1 \end{pmatrix}. \tag{29}$$

Then substituting Equation (6) in Equation (22)

$$\begin{aligned} D_M(\mathbf{m}) &= \frac{|\det M|}{||M^T\mathbf{m}||^4}\frac{1}{\cos^4\theta_{\mathbf{u}}}\frac{1}{\alpha^2}f\left(\frac{\tan\theta_{\mathbf{u}}}{\alpha}\right) \\ &= \frac{\frac{\alpha^2}{\alpha_x\alpha_y}}{\frac{\cos^4\theta_{\mathbf{m}}}{\cos^4\theta_{\mathbf{u}}}}\frac{1}{\cos^4\theta_{\mathbf{u}}}\frac{1}{\alpha^2}f\left(\frac{1}{\alpha}\sqrt{\frac{u_x^2+u_y^2}{u_z^2}}\right) \\ &= \frac{1}{\cos^4\theta_{\mathbf{m}}\alpha_x\alpha_y}f\left(\frac{1}{\alpha}\sqrt{\frac{\alpha^2 m_x^2}{\alpha_x^2 m_z^2}+\frac{\alpha^2 m_y^2}{\alpha_y^2 m_z^2}}\right) \\ &= \frac{1}{\cos^4\theta_{\mathbf{m}}\alpha_x\alpha_y}f\left(\frac{\sin\theta_{\mathbf{m}}}{\cos\theta_{\mathbf{m}}}\sqrt{\frac{\cos^2\phi_{\mathbf{m}}}{\alpha_x^2}+\frac{\sin^2\phi_{\mathbf{m}}}{\alpha_y^2}}\right) \end{aligned} \tag{30}$$

we get to Equation (7) when we first convert $\tan\theta_{\mathbf{u}}$ to cartesian coordinates, express $\mathbf{u}$ in terms of $\mathbf{m}$ from Equation (13) and convert back to spherical coordinates, see Table 1.

An important point is that for shape-variant distributions the scaling of the microsurface is not equivalent to the scaling of the roughness coefficient. Scaling operations of the microsurface are always possible within our framework, while formulas for scaling of the roughness coefficient cannot always be derived.

4.5. Discussion

In summary, for a given microsurface (D, G_1) and a linear transformation M given in Equation (9) our technique defines the transformed microsurface (D_M, G_{1M}) using Equations (22) and (12). It is noteworthy that in our derivation we do not make any assumptions on the input microsurface. Therefore the input distribution can be both shape-invariant and shape-variant, as well as isotropic or anisotropic. This means that it can be used as a *black box* - it can be implemented in a base class and can be applied regardless of the underlying microfacet distribution, including stochastic [JHY*14] or data-driven [APS00; YHJ*14; RBSM19] approaches. Furthermore, the solution is in closed-form and its performance depends mainly on the expressions for D and G_1.

5. Results

We demonstrate our technique using the standard microfacet BRDF for specular microfacets [WMLT07] with an appropriate Fresnel term for dielectrics and conductors. All materials use the GTR distribution with different tail exponents. Dimov derived an accurate Smith shadowing term for GTR tails $\gamma \in [0,4]$ that is exact at the integers [Dim15] which we provide in Appendix A. Due to the lack of sampling formula for the distribution of visible GTR normals the sampling efficiency deteriorates with roughness because of the increased shadowing. We propose a sampling strategy to improve the sampling of rough materials in Appendix B.

5.1. Deforming objects

In Figure 6 we apply our framework in a scene with deforming objects. We track the deformations using a tension texture, based on which we derive the local linear transformations and render the corresponding anisotropic microsurface. The purpose of the tension texture is to compute a 2D tension matrix that contains the local

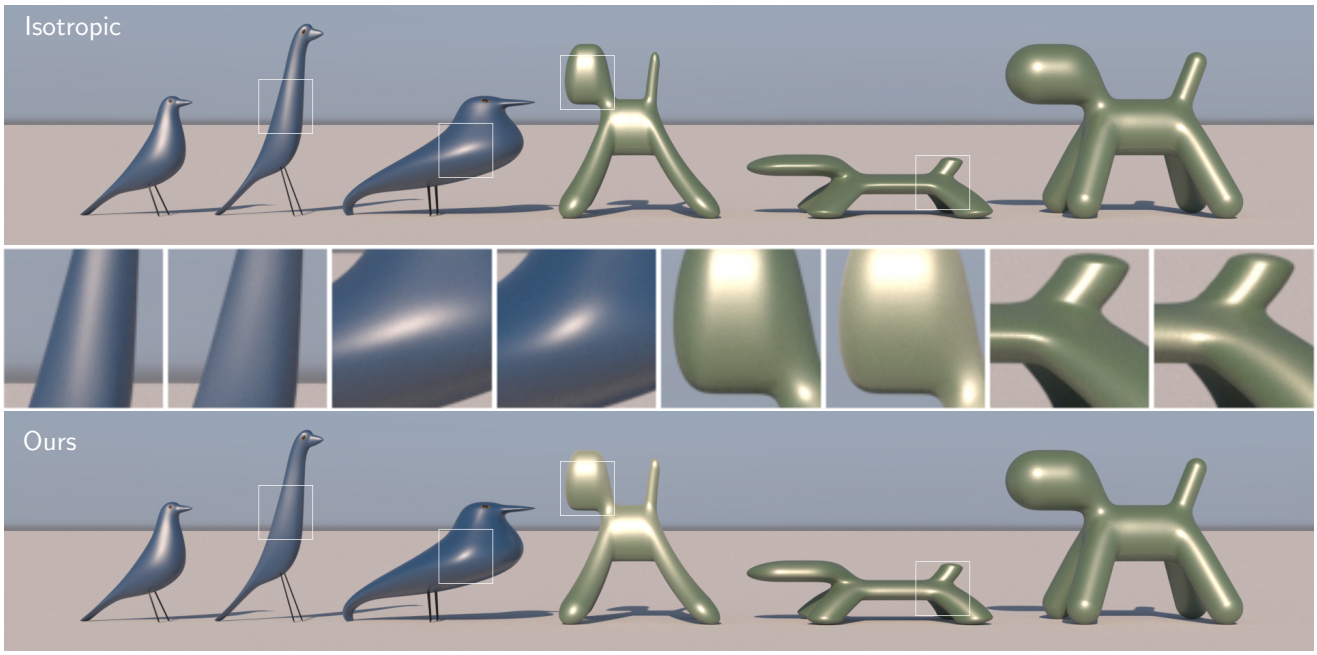

Figure 6: *Decorative objects made from elastic dielectric material with microfacet BRDFs. All birds and all dogs have materials with shape-variant GTR distributions with roughness values* $\alpha = 0.25$ *and* $\alpha = 0.16$*, and tail exponents* $\gamma = 2.2$ *and* $\gamma = 1.4$*, respectively. We demonstrate how the objects reflections change due to deformation. When the object is stretched the microsurface becomes smoother and therefore the reflection highlight becomes sharper. When the microsurface is compressed the reflection spreads out.* ***Top row:*** *A standard isotropic material.* ***Bottom row:*** *Our method that tracks the deformation via a tension matrix and computes the corresponding anisotropic reflection. The first and last objects in the composition are at "rest" state while all objects in between are deformed.* ***Middle row:*** *Alternating zoomed-in regions of isotropic (top row) and deformed anisotropic (bottom row). A helpful analogy to understand the highlight changes that occur with our model is a rubber balloon: as it gets inflated (stretched out), it gets to be smoother and more and more shiny. Our model can replicate this behaviour even for anisotropic stretching.*

surface transformation relative to a predefined “rest” state. In order to compute this, we need a stable local space for each shading point that is consistent between the rest state and the current deformed state of the mesh. Then, at each shading point, we transform the edges of the currently shaded triangle to this local space both for the deformed mesh and for the “rest” mesh. Finally we compute a transformation in local space that converts the “rest” edges to the current deformed edges.

We use the UV mapping coordinates assigned to the surface as the stable local space. For each shading point, we can compute an orthonormal matrix that converts from world space to the local UVW space for the deformed mesh, and another orthonormal matrix that converts from world space to the local UVW space for the “rest” mesh. Using these two matrices, we can rotate the edges of the currently shaded triangle in the deformed mesh and the edges of the same triangle in the "rest" mesh to local space. Note that in general the local UVW spaces are not orthonormal [PJH16] but we force them to be by preserving the U direction and then orthogonalizing and normalizing the matrices. In this way we retain the shape of the triangles and only align them with the U direction in the tangent plane. Let r_1 and r_2 be the transformed edges in local space of the "rest" triangle, and d_1 and d_2 be the transformed edges in local space of the deformed triangle. These edges are 2-dimensional, because we are only interested in the projection to the tangent UV space. Then the 2×2 tension matrix is $T = DR^{-1}$, where $R = (r_1\ r_2)$ and $D = (d_1\ d_2)$, see Figure 7. For shading, we embed the tension matrix in the matrix M, see Equation (9). The tension texture is applied to the deformed object and keeps a reference to the "rest" object. During texture evaluation the matrices R and D are computed for the shaded triangle and the tension matrix T is returned.

This method computes per-face tension matrices and requires relatively fine geometry tessellation to achieve smooth results. Another option is to pre-process the "rest" mesh and the deformed mesh and to store a weighted average of the face tension matrices in the vertices. Upon rendering, vertex tension matrices are interpolated along the triangles to facilitate continuous shading.

5.2. Stretch anisotropy

We have established that traditional anisotropy can be reproduced as a special case of our framework by using a non-uniform scaling matrix, see Equation (29). For our stretch anisotropy we use a convenient scaling transform that is defined by a single scaling factor

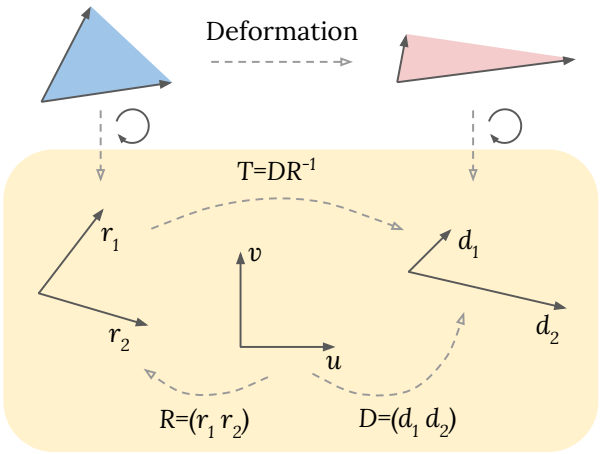

Figure 7: *A triangle of the "rest" mesh (blue) and its corresponding triangle in the deformed mesh (red). The edges of these triangles are rotated to UV space (yellow): the edges of the "rest" triangle r_1 and r_2 form the matrix R that converts to the space of the "rest" triangle, and the edges of the deformed triangle d_1 and d_2 form the matrix D that converts to the space of the deformed triangle. Therefore, the matrix $T = DR^{-1}$ encodes the local tension of the deformation.*

$s \in (-1,1)$:

$$M_s = \begin{cases} diag\left(\frac{1}{1-s}, 1-s, 1\right), & s \in [0,1) \\ diag\left(1+s, \frac{1}{1+s}, 1\right), & s \in (-1,0) \end{cases}. \tag{31}$$

For positive values of s it stretches the x-coordinate and shrinks the y-coordinate while for negative values of s it does the opposite. Moreover, $\det M_s = 1$, $M_s^T = M_s$, $M_0 = I$ and M_s^{-1} is constructed by swapping the first two diagonal entries of M_s. Note that a 2D rotation can be concatenated with the matrix M_s, but we choose to keep the matrix simple, and perform anisotropy rotation via the shading frame rotation.

We showcase our technique in Figure 8. The vases have brushed aluminum material, and all of them have anisotropic shape-variant distributions that do not have analytic elliptical anisotropic equations, given in Equation (5).

6. Conclusion

We propose a change in how one goes about the construction of anisotropic microfacet distributions. Performing these derivations based on the transformations that need to be done to the microgeometry, instead of based on the directional variation of surface roughness, offers desirable advantages: our approach works with all planar linear transformations (including skew), and with all slope distribution functions, regardless of whether they are shape-invariant, or not. This offers artists a wider range of creative control, both in terms of the highlight shapes they can create, and the types of surfaces that can be made anisotropic.

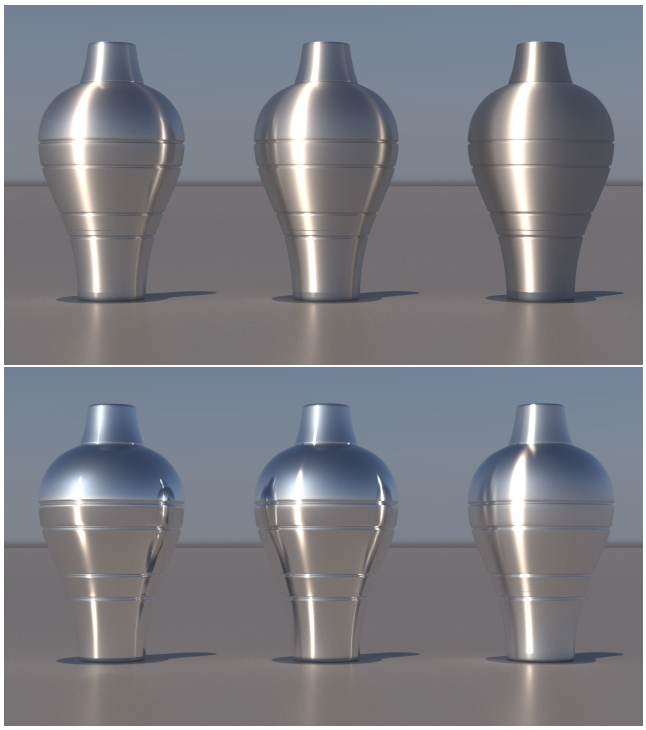

Figure 8: *Brushed aluminum vases rendered with GTR distribution. Columns from left to right have roughness values $\alpha = 0.01, 0.04, 0.16$. The top row has the Berry distribution $\gamma = 1$ and the bottom row has a tail exponent $\gamma = 3.5$. All materials have shape-variant anisotropic distributions with scaling factor $s = \frac{5}{2}$, see Equation (31).*

7. Acknowledgements

We thank members from Chaos Bulgaria R&D team for proofreading the manuscript and the anonymous reviewers for constructive feedback. We also acknowledge funding from Charles University grant SVV-260588 and the Czech Science Foundation (GAČR) grant 22-22875S.

References

[AK16] ATANASOV, ASEN and KOYLAZOV, VLADIMIR. "A Practical Stochastic Algorithm for Rendering Mirror-like Flakes". *ACM SIGGRAPH 2016 Talks*. SIGGRAPH '16. Anaheim, California: Association for Computing Machinery, 2016. ISBN: 9781450342827. DOI: 10.1145/2897839.2927391. URL: https://doi.org/10.1145/2897839.2927391 3, 7.

[APS00] ASHIKMIN, MICHAEL, PREMOŽE, SIMON, and SHIRLEY, PETER. "A Microfacet-Based BRDF Generator". *Proceedings of the 27th Annual Conference on Computer Graphics and Interactive Techniques*. SIGGRAPH '00. USA: ACM Press/Addison-Wesley Publishing Co., 2000, 65–74. ISBN: 1581132085. DOI: 10.1145/344779.344814. URL: https://doi.org/10.1145/344779.344814 2, 3, 7.

[Ber23] BERRY, EUGENE M. "Diffuse Reflection of Light from a Matt Surface". *J. Opt. Soc. Am.* 7.8 (Aug. 1923), 627–633. DOI: 10.1364/JOSA.7.000627. URL: http://opg.optica.org/abstract.cfm?URI=josa-7-8-627 3, 11.

[Bli77] BLINN, JAMES F. "Models of Light Reflection for Computer Synthesized Pictures". *SIGGRAPH Comput. Graph.* 11.2 (July 1977), 192–198. ISSN: 0097-8930. DOI: 10.1145/965141.563893. URL: https://doi.org/10.1145/965141.563893 2.

[BLPW14] BRADY, ADAM, LAWRENCE, JASON, PEERS, PIETER, and WEIMER, WESTLEY. "GenBRDF: Discovering New Analytic BRDFs with Genetic Programming". *ACM Trans. Graph.* 33.4 (July 2014). ISSN: 0730-0301. DOI: 10.1145/2601097.2601193. URL: https://doi.org/10.1145/2601097.2601193 3.

[BM14] BUTLER, SAMUEL D. and MARCINIAK, MICHAEL A. "Robust categorization of microfacet BRDF models to enable flexible application-specific BRDF adaptation". *Reflection, Scattering, and Diffraction from Surfaces IV*. Ed. by HANSSEN, LEONARD M. Vol. 9205. Society of Photo-Optical Instrumentation Engineers (SPIE) Conference Series. Sept. 2014, 920506, 920506. DOI: 10.1117/12.2061134 3.

[BPV18] BARLA, PASCAL, PACANOWSKI, ROMAIN, and VANGORP, PETER. "A Composite BRDF Model for Hazy Gloss". *Comput. Graph. Forum* 37.4 (2018), 55–66. DOI: 10.1111/cgf.13475. URL: https://doi.org/10.1111/cgf.13475 3.

[BS63] BECKMANN, PETR and SPIZZICHINO, ANDRE. *The Scattering of Electromagnetic Waves from Rough Surfaces*. New York: Pergamon, 1963 2.

[Bur12] BURLEY, BRENT. "Physically-Based Shading at Disney". 2012 2–4, 7, 11.

[CT82] COOK, R. L. and TORRANCE, K. E. "A Reflectance Model for Computer Graphics". *ACM Trans. Graph.* 1.1 (Jan. 1982), 7–24. ISSN: 0730-0301. DOI: 10.1145/357290.357293. URL: http://doi.acm.org/10.1145/357290.357293 2.

[dBoo01] De BOOR, C. *A Practical Guide to Splines*. Applied Mathematical Sciences. Springer New York, 2001. ISBN: 9780387953663. URL: https://books.google.bg/books?id=m0QDJvBI%5C_ecC 11.

[DHI*13] DUPUY, JONATHAN, HEITZ, ERIC, IEHL, JEAN-CLAUDE, et al. "Linear Efficient Antialiased Displacement and Reflectance Mapping". *ACM Transactions on Graphics*. Proceedings of Siggraph Asia 2013 32.6 (Nov. 2013), Article No. 211. DOI: 10.1145/2508363.2508422. URL: https://hal.inria.fr/hal-00858220 2.

[DHI*15] DUPUY, JONATHAN, HEITZ, ERIC, IEHL, JEAN-CLAUDE, et al. "Extracting Microfacet-based BRDF Parameters from Arbitrary Materials with Power Iterations". *Computer Graphics Forum* (2015), 10. URL: https://hal.inria.fr/hal-01168516 2.

[Dim15] DIMOV, ROSSEN. "Deriving the Smith shadowing function G_1 for $\gamma \in (0,4]$". 2015 7, 11.

[EK17] ESTEVEZ, ALEJANDRO CONTY and KULLA, CHRISTOPHER. "Production Friendly Microfacet Sheen BRDF". 2017 3, 7.

[HD14] HEITZ, ERIC and D'EON, EUGENE. "Importance Sampling Microfacet-Based BSDFs using the Distribution of Visible Normals". *Computer Graphics Forum* 33.4 (July 2014), 103–112. DOI: 10.1111/cgf.12417. URL: https://hal.inria.fr/hal-00996995 2, 7, 11.

[HDHN16] HEITZ, ERIC, DUPUY, JONATHAN, HILL, STEPHEN, and NEUBELT, DAVID. "Real-Time Polygonal-Light Shading with Linearly Transformed Cosines". *ACM Trans. Graph.* 35.4 (July 2016). ISSN: 0730-0301. DOI: 10.1145/2897824.2925895. URL: https://doi.org/10.1145/2897824.2925895 3, 6.

[Hei14] HEITZ, ERIC. "Understanding the Masking-Shadowing Function in Microfacet-Based BRDFs". *Journal of Computer Graphics Techniques (JCGT)* 3.2 (June 2014), 48–107. ISSN: 2331-7418. URL: http://jcgt.org/published/0003/02/03/ 2–5, 7.

[HG41] HENYEY, L. G. and GREENSTEIN, J. L. "Diffuse radiation in the Galaxy." *Astrophysical Journal* 93 (Jan. 1941), 70–83. DOI: 10.1086/144246 3.

[HHdD16] HEITZ, ERIC, HANIKA, JOHANNES, D'EON, EUGENE, and DACHSBACHER, CARSTEN. "Multiple-Scattering Microfacet BSDFs with the Smith Model". *ACM Trans. Graph.* 35.4 (July 2016). ISSN: 0730-0301. DOI: 10.1145/2897824.2925943. URL: https://doi.org/10.1145/2897824.2925943 2, 5.

[HP17] HOLZSCHUCH, NICOLAS and PACANOWSKI, ROMAIN. "A Two-Scale Microfacet Reflectance Model Combining Reflection and Diffraction". *ACM Transactions on Graphics* 36.4 (July 2017). Article 66, 12. DOI: 10.1145/3072959.3073621. URL: https://hal.inria.fr/hal-01515948 2.

[HSRG07] HAN, CHARLES, SUN, BO, RAMAMOORTHI, RAVI, and GRINSPUN, EITAN. "Frequency domain normal map filtering". *ACM Trans. Graph.* 26 (July 2007), 28. DOI: 10.1145/1275808.1276412 2.

[JHY*14] JAKOB, WENZEL, HAŠAN, MILOŠ, YAN, LING-QI, et al. "Discrete Stochastic Microfacet Models". *ACM Trans. Graph.* 33.4 (July 2014). ISSN: 0730-0301. DOI: 10.1145/2601097.2601186. URL: https://doi.org/10.1145/2601097.2601186 2, 7.

[Kaj85] KAJIYA, JAMES T. "Anisotropic Reflection Models". *SIGGRAPH Comput. Graph.* 19.3 (July 1985), 15–21. ISSN: 0097-8930. DOI: 10.1145/325165.325167. URL: https://doi.org/10.1145/325165.325167 2.

[KSK10] KURT, MURAT, SZIRMAY-KALOS, LÁSZLÓ, and KŘIVÁNEK, JAROSLAV. "An Anisotropic BRDF Model for Fitting and Monte Carlo Rendering". *SIGGRAPH Comput. Graph.* 44.1 (Feb. 2010). ISSN: 0097-8930. DOI: 10.1145/1722991.1722996. URL: https://doi.org/10.1145/1722991.1722996 2.

[LKYU12] LÖW, JOAKIM, KRONANDER, JOEL, YNNERMAN, ANDERS, and UNGER, JONAS. "BRDF Models for Accurate and Efficient Rendering of Glossy Surfaces". *ACM Trans. Graph.* 31.1 (Feb. 2012). ISSN: 0730-0301. DOI: 10.1145/2077341.2077350. URL: https://doi.org/10.1145/2077341.2077350 3.

[NFA*15] NAGANO, KOKI, FYFFE, GRAHAM, ALEXANDER, OLEG, et al. "Skin Microstructure Deformation with Displacement Map Convolution". *ACM Trans. Graph.* 34.4 (July 2015). ISSN: 0730-0301. DOI: 10.1145/2766894. URL: https://doi.org/10.1145/2766894 2.

[NVZJ19] NIMIER-DAVID, MERLIN, VICINI, DELIO, ZELTNER, TIZIAN, and JAKOB, WENZEL. "Mitsuba 2: A Retargetable Forward and Inverse Renderer". *ACM Trans. Graph.* 38.6 (Nov. 2019). ISSN: 0730-0301. DOI: 10.1145/3355089.3356498. URL: https://doi.org/10.1145/3355089.3356498 2.

[PF90] POULIN, PIERRE and FOURNIER, ALAIN. "A Model for Anisotropic Reflection". *SIGGRAPH Comput. Graph.* 24.4 (Sept. 1990), 273–282. ISSN: 0097-8930. DOI: 10.1145/97880.97909. URL: https://doi.org/10.1145/97880.97909 2.

[PJH16] PHARR, MATT, JAKOB, WENZEL, and HUMPHREYS, GREG. *Physically Based Rendering: From Theory to Implementation (3rd ed.)* 3rd. San Francisco, CA, USA: Morgan Kaufmann Publishers Inc., Nov. 2016, 1266. ISBN: 9780128006450 2, 5, 6, 8.

[RBMS17] RIBARDIÈRE, MICKAËL, BRINGIER, BENJAMIN, MENEVEAUX, DANIEL, and SIMONOT, LIONEL. "STD: Student's t-Distribution of Slopes for Microfacet Based BSDFs". *Computer Graphics Forum* 36.2 (2017). DOI: 10.1111/cgf.13137. URL: https://hal.archives-ouvertes.fr/hal-01535614 3, 7.

[RBSM19] RIBARDIÈRE, MICKAËL, BRINGIER, BENJAMIN, SIMONOT, LIONEL, and MENEVEAUX, DANIEL. "Microfacet BSDFs Generated from NDFs and Explicit Microgeometry". *ACM Trans. Graph.* 38.5 (June 2019). ISSN: 0730-0301. DOI: 10.1145/3338697. URL: https://doi.org/10.1145/3338697 2, 3, 7.

[RDP05] ROSS, VINCENT, DION, DENIS, and POTVIN, GUY. "Detailed analytical approach to the Gaussian surface bidirectional reflectance distribution function specular component applied to the sea surface". *J. Opt. Soc. Am. A* 22.11 (Nov. 2005), 2442–2453. DOI: 10.1364/JOSAA.22.002442. URL: http://opg.optica.org/josaa/abstract.cfm?URI=josaa-22-11-2442 4.

[Smi67] SMITH, B. "Geometrical shadowing of a random rough surface". *IEEE Transactions on Antennas and Propagation* 15.5 (1967), 668–671. DOI: 10.1109/TAP.1967.1138991 2, 3.

[TR75] TROWBRIDGE, T. S. and REITZ, K. P. "Average irregularity representation of a rough surface for ray reflection". *J. Opt. Soc. Am.* 65.5 (May 1975), 531–536. DOI: 10.1364/JOSA.65.000531. URL: http://www.osapublishing.org/abstract.cfm?URI=josa-65-5-531 2.

[TS67] TORRANCE, K.E. and SPARROW, E.M. "Theory for Off-Specular Reflection from Roughened Surfaces". *Journal of the Optical Society of America (JOSA)* 57.9 (Sept. 1967), 1105–1114. URL: http://www.graphics.cornell.edu/~westin/pubs/TorranceSparrowJOSA1967.pdf 2, 3.

[VG95] VEACH, ERIC and GUIBAS, LEONIDAS J. "Optimally Combining Sampling Techniques for Monte Carlo Rendering". *Proceedings of the 22nd Annual Conference on Computer Graphics and Interactive Techniques*. SIGGRAPH '95. New York, NY, USA: ACM, 1995, 419–428. ISBN: 0-89791-701-4. DOI: 10.1145/218380.218498. URL: http://doi.acm.org/10.1145/218380.218498 11.

[War92] WARD, GREGORY J. "Measuring and Modeling Anisotropic Reflection". *SIGGRAPH Comput. Graph.* 26.2 (July 1992), 265–272. ISSN: 0097-8930. DOI: 10.1145/142920.134078. URL: https://doi.org/10.1145/142920.134078 2.

[WDR11] WU, HONGZHI, DORSEY, JULIE, and RUSHMEIER, HOLLY. "Physically-Based Interactive Bi-Scale Material Design". *ACM Trans. Graph.* 30.6 (Dec. 2011), 1–10. ISSN: 0730-0301. DOI: 10.1145/2070781.2024179. URL: https://doi.org/10.1145/2070781.2024179 2.

[WMLT07] WALTER, BRUCE, MARSCHNER, STEPHEN R., LI, HONGSONG, and TORRANCE, KENNETH E. "Microfacet Models for Refraction Through Rough Surfaces". *Proceedings of the 18th Eurographics Conference on Rendering Techniques*. EGSR'07. Grenoble, France: Eurographics Association, 2007, 195–206. ISBN: 978-3-905673-52-4. DOI: 10.2312/EGWR/EGSR07/195-206. URL: http://dx.doi.org/10.2312/EGWR/EGSR07/195-206 2–4, 7, 11.

[WOB*06] WELLEMS, DAVID, ORTEGA, STEVE, BOWERS, DAVID, et al. "Long wave infrared polarimetric model: theory, measurements and parameters". *Journal of Optics A: Pure and Applied Optics* 8.10 (Oct. 2006), 914–925. DOI: 10.1088/1464-4258/8/10/014 3.

[Wol16] WOLFRAM RESEARCH, INC. *Mathematica, Version 10.4*. Champaign, IL. 2016. URL: https://www.wolfram.com/mathematica 6.

[WZYR19] WU, LIFAN, ZHAO, SHUANG, YAN, LING-QI, and RAMAMOORTHI, RAVI. "Accurate Appearance Preserving Prefiltering for Rendering Displacement-Mapped Surfaces". *ACM Trans. Graph.* 38.4 (July 2019). ISSN: 0730-0301. DOI: 10.1145/3306346.3322936. URL: https://doi.org/10.1145/3306346.3322936 2.

[YHJ*14] YAN, LING-QI, HAŠAN, MILOŠ, JAKOB, WENZEL, et al. "Rendering Glints on High-Resolution Normal-Mapped Specular Surfaces". *ACM Transactions on Graphics (Proceedings of SIGGRAPH)* 33.4 (July 2014), 116:1–116:9. DOI: 10.1145/2601097.2601155 2, 7.

Appendix A: A Smith shadowing term for GTR $\gamma \in [0,4]$, which is exact for the integer tails

Burley [Bur12] introduced the isotropic GTR distribution

$$D_\gamma(\mathbf{m}) = \frac{(\gamma-1)(\alpha^2-1)}{\pi(1-(\alpha^2)^{1-\gamma})} \frac{1}{(1+(\alpha^2-1)\cos^2\theta_\mathbf{m})^\gamma}, \tag{32}$$

where $\alpha \in [0,1]$ controls the roughness and $\gamma \geq 0$ is the tail exponent. The distribution has a $\frac{0}{0}$ singularity at $\gamma = 1$, and it converges to the Berry distribution [Ber23; Bur12] at the limit

$$D_1(\mathbf{m}) = \lim_{\gamma \to 1} D_\gamma(\mathbf{m}) = \frac{(\alpha^2-1)}{\pi \log \alpha^2} \frac{1}{(1+(\alpha^2-1)\cos^2\theta_\mathbf{m})}. \tag{33}$$

A plot of the GTR distribution for a fixed roughness $\alpha = 0.6$ and tails $\gamma \in \{0,1,2,3,4\}$ is presented in Figure 9 a).

Dimov [Dim15] followed the derivation procedure of Smith shadowing that is described by Walter et al. [WMLT07]. With this approach he was not able to find a general analytic formula $G_{1\gamma}$, perhaps due to the singularity at $\gamma = 1$. Fortunately, he found analytic formulas for a few special values - $\gamma \in \{0,1,3,4\}$. Here we express these results in terms of the average visibility $S_\gamma(\mu)$, with $\mu = |\cot\theta_\mathbf{v}|$, where the monodirectional shadowing formula is

$$G_{1\gamma}(\mathbf{v},\mathbf{m}) = \chi^+\left(\frac{\mathbf{v}\cdot\mathbf{m}}{\mathbf{v}\cdot\mathbf{n}}\right) S_\gamma(\mu) \tag{34}$$

[WMLT07]. Follows a list of formulas for the GTR average visibility for integer tails, including the GGX average visibility S_2 for completeness:

$$S_0(\mu) = \frac{2}{1+\sqrt{\frac{1}{\mu^2}+1}}, \tag{35}$$

$$S_1(\mu) = \frac{\mu \log \alpha^2}{A_1 - B_1 + \mu \log\left(\frac{\alpha^2(\mu+B_1)}{\mu+A_1}\right)}, \tag{36}$$

where $A_1 = \sqrt{\mu^2+\alpha^2}$ and $B_1 = \sqrt{\mu^2+1}$,

$$S_2(\mu) = \frac{2}{1+\sqrt{\frac{\alpha^2}{\mu^2}+1}}, \tag{37}$$

$$S_3(\mu) = \frac{4B_3\mu A_3}{\alpha^2(3\alpha^2+1)+2\mu B_3(\mu+A_3)}, \tag{38}$$

where $A_3 = \sqrt{\mu^2+\alpha^2}$ and $B_3 = \alpha^2+1$ and

$$S_4(\mu) = \frac{2A_4\mu B_4^3}{A_4\mu(B_4^3+\mu^3)+3\alpha^2(\alpha^2(5\alpha^4+2\alpha^2+1)+4\mu^2(2\alpha^4+\alpha^2+1))}, \tag{39}$$

where $A_4 = 8\alpha^4+8\alpha^2+8$ and $B_4 = \sqrt{\mu^2+\alpha^2}$.

In Figure 9 b) we show these shadowing curves for a fixed roughness $\alpha = 0.6$. In order to compute an accurate approximation for all non-integer tails $\gamma \in (0,4)$ all five integer formulas are evaluated and a cubic spline interpolation [dBoo01] is performed. Natural boundary conditions are suggested in order to minimize the oscillations. We have verified that with this approach the constraint in Equation (2) is closely met.

Appendix B: An improved sampling for the GTR distribution

Rendering microfacet BRDF with GTR distribution with high roughness has inherent high variance due to the lack of sampling equations from the distribution of visible normals [HD14]. The reduced effectiveness of the sampling from D [WMLT07] is due to increased shadowing. When the roughness is approaching 1 the single scattering term gets darker and more diffuse. We found that stochastic mixing of the sampling strategy with uniform sampling improves the sampling of rough surfaces. A random number and the roughness α determine whether uniform sampling or sampling from D will be used for the direction. The balance heuristic is finally applied for probability computation[VG95]. Render time comparison can be seen in Figure 10.

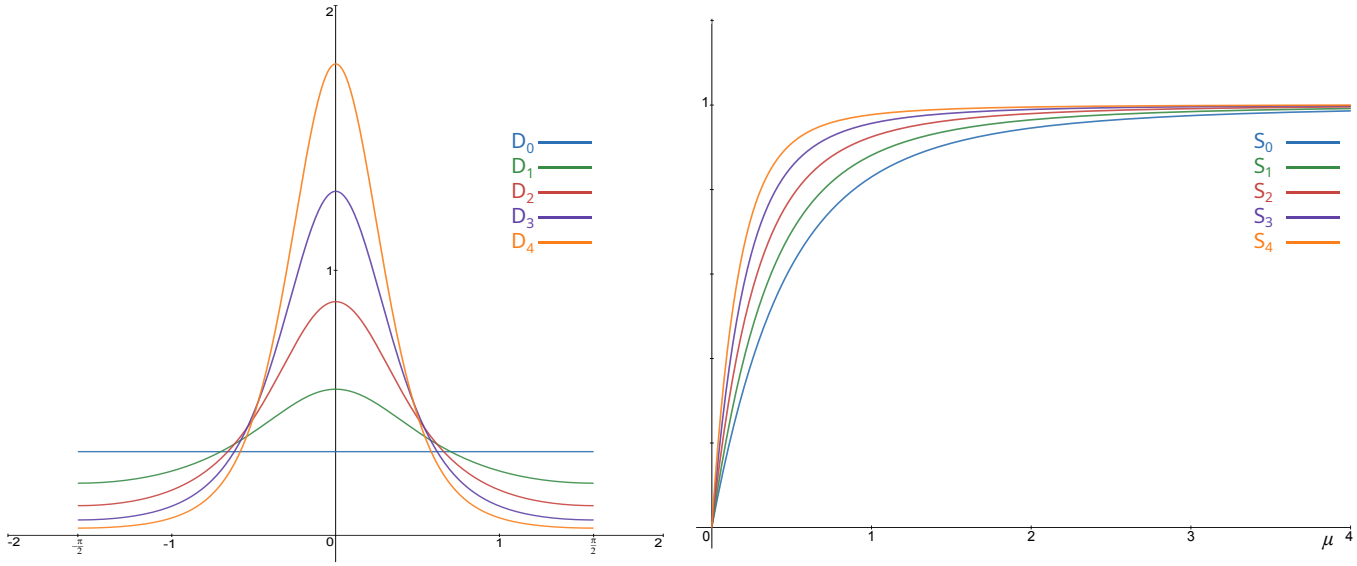

a) GTR Microfacet distribution D_γ b) GTR Average visibility S_γ

Figure 9: *Plots of the microfacet distribution D_γ and the average visibility S_γ for $\gamma = \{0,1,2,3,4\}$ and for a fixed roughness α =0.6. Note that $\lim_{\alpha\to 0,\gamma>0}(D_\gamma,S_\gamma) = (\delta,1)$ and $\lim_{\alpha\to 1}(D_\gamma,S_\gamma) = (D_0,S_0)$.*

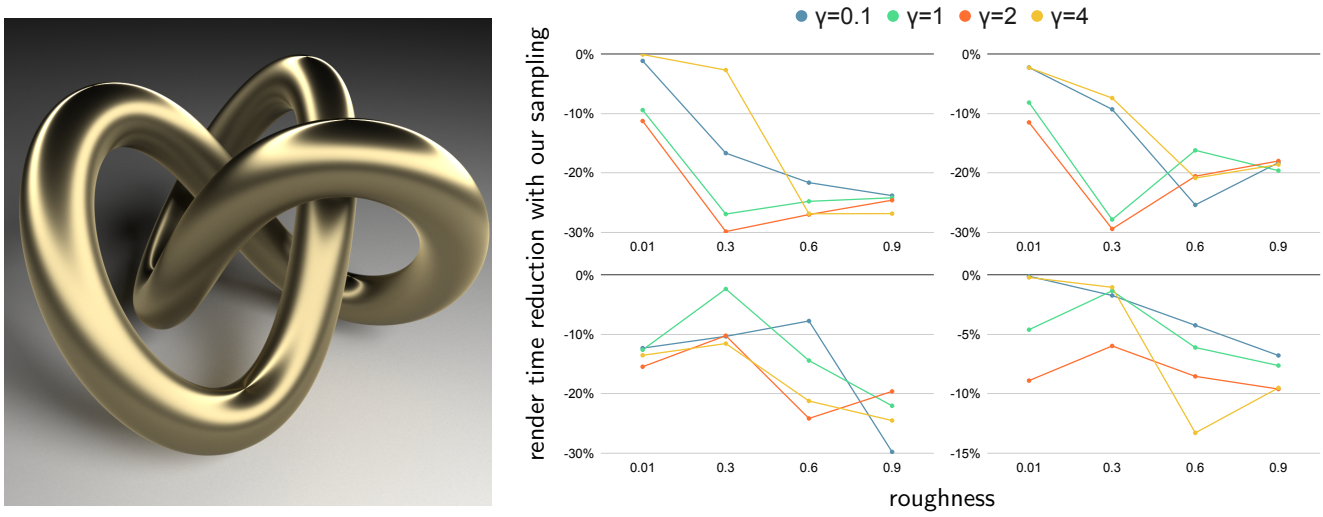

Figure 10: ***Left:*** *Torus knot with GTR roughness $\alpha = 0.3$, tail exponent $\gamma = 1$ and anisotropy $s = 0.75$, lit by a rectangular light.* ***Right:*** *Charts for the torus knot scene showing how much render times improve for the same image quality when switching from classic sampling to our sampling described in Appendix B. We use variance-based image sampler which samples each pixel until a given noise level is reached. Top left chart is for isotropic material ($s = 0$) with 95 average samples per pixel (aspp) for the classical sampling vs. 84 aspp for our sampling. The top right, bottom left and bottom right charts represent anisotropic materials with $s = \{0.25,\ 0.5,\ 0.75\}$ and 91 vs. 79 aspp, 95 vs. 89 aspp and 131 vs. 119 aspp, respectively. Therefore, our sampling technique reduces the number of samples per pixel by 10% on average for this scene. Moreover, the charts demonstrate that this technique helps with very different distribution tails: GTR with $\gamma = 0.1$ has much heavier tail than GGX while the tail of GTR with $\gamma = 4$ is much "lighter", see Figure 9 a).*